PHOTONIC SENSORS / Vol. 8, No. 2, 2018: 176–187

Propagation of Electromagnetic Waves in Slab Waveguide Structure Consisting of Chiral Nihility Claddings and Negative-Index Material Core Layer

Alaa N. Abu HELAL, Sofyan A. TAYA*, and Khitam Y. ELWASIFE

Physics Department, Islamic University of Gaza, Gaza, 108, Palestine

*Corresponding author: Sofyan A. TAYA Email: staya@iugaza.edu.ps

Abstract: The dispersion equation of an asymmetric three-layer slab waveguide, in which all layers are chiral materials is presented. Then, the dispersion equation of a symmetric slab waveguide, in which the claddings are chiral materials and the core layer is negative index material, is derived. Normalized cut-off frequencies, field profile, and energies flow of right-handed and left-handed circularly polarized modes are derived and plotted. We consider both odd and even guided modes. Numerical results of guided low-order modes are provided. Some novel features, such as abnormal dispersion curves, are found.

Keywords: Slab waveguides; chiral materials; left-handed materials

Citation: Alaa N. Abu HELAL, Sofyan A. TAYA, and Khitam Y. ELWASIFE, "Propagation of Electromagnetic Waves in Slab Waveguide Structure Consisting of Chiral Nihility Claddings and Negative-Index Material Core Layer," *Photonic Sensors*, 2018, 8(2): 176–187.

1. Introduction

Left-handed materials (LHMs), also known as negative-index materials (NIMs), were demonstrated theoretically in 1968 by Veselago [1]. These double negative materials with simultaneously negative electric permittivity (ε) and magnetic permeability (μ) have abnormal properties, such as a negative index of refraction, sub wavelength imaging, backward wave propagation, and reverse Doppler and Cherenkov effects [1–22]. These materials cannot be found in nature but are man-made. Because of their novel properties, Pendry and his co-authors worked hard to generate NIM and finally developed the concept of a perfect lens [9]. The main idea to fabricate NIMs is to treat the permittivity and permeability separately. Pendry used wire array structure to generate negative permittivity and split-ring resonator (SRR) structure to generate negative permeability [11, 13]. At the time when it was quite difficult to obtain a negative refractive index of refraction in the visible region, Shelby experimentally fabricated the first NIM in the microwave region [23]. More and more attention to this kind of metamaterial has been drawn due to its abnormal properties and possible applications in many fields such as cloaking [24], micro strip patch antenna [25], wave absorbers [26], and biochemical sensors [27–36].

A material with high optical activity can also have a negative index of refraction. This property makes a material capable of revolving the plane of

Received: 22 March 2017 / Revised: 25 January 2018

DOI: 10.1007/s13320-018-0414-z
Article type: Regular

incident polarized light due to the asymmetrical molecular structure. In the beginning of 19th century, chiral media were discovered and studied due to their optical activity. At the interface between the chiral material and achiral material, bi-refraction occurs because of the existence of two different modes caused by the chiral medium. A chiral medium can have a negative index of refraction. If the chirality coefficient (κ) is strong and greater than the index of refraction at least near the resonant frequency, one eigen-wave in the chiral medium turns out to be a backward wave, and the phenomenon of negative refraction in the chiral material occurs. Therefore, chiral materials can achieve negative refraction, from which we call chiral negative refractive index medium [37].

The Greek word "chiral" means "hand": our hands are mirror images and they cannot be superimposed on each other no matter how hard we try. A chiral object cannot be superimposed on its mirror image neither by translation nor by rotation. The modes in a chiral bulk material can be divided into right-handed circular polarization (RCP) and left-handed circular polarization (LCP). When a linearly polarized light propagates through a chiral material, it is decomposed into two orthogonal modes known as RCP and LCP. Upon leaving the chiral medium, the two modes recombine again, and the output is linearly polarized. The effect of the chiral medium is to rotate the plane of polarization with an angle depending on the thickness of the chiral material. Due to the novel features of chiral media, intensive interest has been focused on waveguide structures comprising chiral materials [38–43]. Waveguide structures comprising chiral media were first studied by P. Pelet [38]. They have unique propagating properties such as hybrid modes.

In this work, the properties of guided modes in slab waveguides in which the claddings are chiral nihility and the core is left-handed metamaterial are investigated theoretically. The characteristic equations, field profile, and energy flow in the waveguide layers of several low-order guided modes in the chiral nihility waveguide structure are presented. Some unusual properties such as abnormal dispersion behavior in the chiral nihility waveguide are observed.

2. Theory of chiral materials

2.1 Dispersion relations of slab chiral waveguides

The structure of an asymmetric three-layer slab chiral waveguide is shown in Fig. 1. The film has a permittivity ε_2, permeability μ_2, chirality κ_2, and thickness d. Regions 1 and 3 are semi-infinite chiral materials with different refractive indexes and chirality. The electric and magnetic fields in the chiral material are coupled because of the chirality parameter.

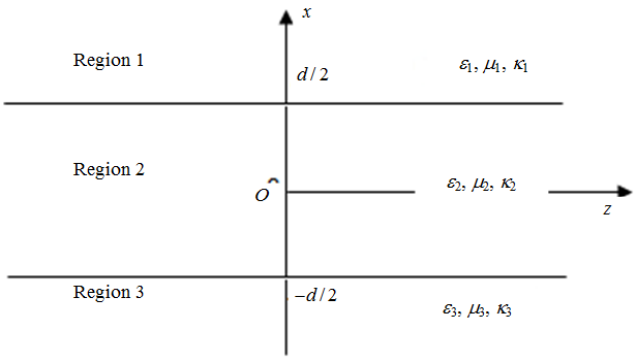

Fig. 1 Schematic diagram of three-layer waveguide structure having chiral materials.

The constitutive relations for the chiral media can be written as

$$D = \varepsilon_i E - \mathrm{j}\kappa_i \sqrt{\varepsilon_0 \mu_0}\, H,\ B = \mu_i H + \mathrm{j}\kappa_i \sqrt{\varepsilon_0 \mu_0}\, E \quad (1)$$

where E, H, D, and B are the electric field, magnetic field, electric displacement, and magnetic flux density, respectively.

In the chiral material, electric and magnetic fields can be written as follows:

$$E = E_+ + E_-,\ \ H = H_+ + H_-. \quad (2)$$

The magnetic fields in chiral material are related to the electric fields through

$$H_{\pm} = \pm \mathrm{j} \cdot E_{\pm} / \eta_i \tag{3}$$

where the (±) symbols correspond to the RCP and LCP waves in the chiral medium, respectively. $\eta_i = \sqrt{\mu_i / \varepsilon_i}$ is the wave impedance in the medium *i*. Substitution (2) and (3) into Maxwell's equations for source-free regions yealds the wave equations for RCP and LCP fields as

$$\left(\nabla^2 + k_{i\pm}^2\right) E_{\pm y} = 0 \tag{4}$$

where $k_{i\pm} = k_0 \left(n_i \pm \kappa_i\right)$, $k_0 = \omega\sqrt{\varepsilon_0 \mu_0}$, and $n_i = \sqrt{\mu_i \varepsilon_i / \mu_0 \varepsilon_0}$ are effective refractive indexes of the two eigen-waves, the wave number in free space, and the refractive index of the chiral medium. We consider the z dependence of the fields is $\exp\left(-\mathrm{j}\beta z\right)$.

Define the parameters $\gamma_{\pm}$, $\delta_{\pm}$, and $\alpha_{\pm}$ as $\gamma_{\pm} = (\beta^2 - k_{1\pm}^2)^{1/2}$, $\delta_{\pm} = (k_{2\pm}^2 - \beta^2)^{1/2}$, and $\alpha_{\pm} = (\beta^2 - k_{3\pm^2})^{1/2}$. The solutions of the longitudinal-field component in (4) and derivation of the dispersion relation are shown in Appendix A.

Next, we will study the dispersion equations of guided modes in a three-layer symmetric slab chiral waveguide. When the structure shown in Fig. 1 becomes symmetric, i.e., Region 1 and Region 3 have the same refractive index and chirality $\kappa_1 = \kappa_3$, $\varepsilon_1 = \varepsilon_3$, and $\mu_1 = \mu_3$, the solutions of the longitudinal-field component in (4) are shown again in Appendix A.

Other components of the fields are obtained, the continuity conditions are applied, and we obtain the following dispersion relations as

$$\frac{4k_{2+}k_{2-}}{\delta_+\delta_-}\cos u_+ \cos u_- + \frac{4k_{1+}k_{1-}}{\gamma_+\gamma_-}\sin u_+ \sin u_- - \frac{1}{\eta_1\eta_2} \times \left\{\left[\frac{k_{1+}k_{2+}}{\delta_+\gamma_+}(\eta_1 - \eta_2)^2 + \frac{k_{1-}k_{2+}}{\delta_+\gamma_-}(\eta_1 + \eta_2)^2\right]\sin u_- \cos u_+ + \left[\frac{k_{1-}k_{2-}}{\delta_-\gamma_-}(\eta_1 - \eta_2)^2 + \frac{k_{1+}k_{2-}}{\delta_-\gamma_+}(\eta_1 + \eta_2)^2\right]\cos u_- \sin u_+\right\} = 0 \tag{5}$$

for odd guided modes and

$$\frac{4k_{1+}k_{1-}}{\gamma_+\gamma_-}\cos u_+ \text{ relations } \cos u_- + \frac{4k_{2+}k_{2-}}{\delta_+\delta_-}\sin u_+ \sin u_- + \frac{1}{\eta_1\eta_2} \times \left\{\left[\frac{k_{1+}k_{2-}}{\delta_-\gamma_+}(\eta_1 + \eta_2)^2 + \frac{k_{1-}k_{2-}}{\delta_-\gamma_-}(\eta_1 - \eta_2)^2\right]\sin u_- \cos u_+ + \left[\frac{k_{1-}k_{2+}}{\delta_+\gamma_-}(\eta_1 + \eta_2)^2 + \frac{k_{1+}k_{2+}}{\delta_+\gamma_+}(\eta_1 - \eta_2)^2\right]\cos u_- \sin u_+\right\} = 0 \tag{6}$$

for even guided modes.

2.2 Dispersion of three-layer symmetric slab achiral core and chiral cladding waveguides

When the geometry of the waveguide consists of an achiral core and chiral claddings, where $\kappa_2 = 0$, the above parameters become $k_{1\pm} = k_0\left(n_1 \pm \kappa_1\right)$, $k_{2\pm} = n_2 k_0 = k_2$, $\gamma_{\pm} = (\beta^2 - k_{1\pm}^2)^{1/2}$, and $\delta_{\pm} = (k_2^2 - \beta^2)^{1/2} = \delta$, and the characteristics (5) and (6) can be written as

$$\frac{2k_0^2\left(n_1^2 - \kappa_1^2\right)}{\gamma_+\gamma_-}\sin^2 u + \frac{2k_2^2}{\delta^2}\cos^2 u - \frac{k_2\left(\eta_1^2 + \eta_2^2\right)}{\delta\eta_1\eta_2}\sin u \cos u\left\{\left(\frac{k_{1+}}{\gamma_+}\right) + \left(\frac{k_{1-}}{\gamma_-}\right)\right\} = 0 \tag{7}$$

for odd guided modes and

$$\frac{2k_0^2\left(n_1^2 - \kappa_1^2\right)}{\gamma_+\gamma_-}\cos^2 u + \frac{2k_2^2}{\delta^2}\sin^2 u + \frac{k_2\left(\eta_1^2 + \eta_2^2\right)}{\delta\eta_1\eta_2}\sin u \cos u\left\{\left(\frac{k_{1+}}{\gamma_+}\right) + \left(\frac{k_{1-}}{\gamma_-}\right)\right\} = 0 \tag{8}$$

for even guided modes.

When the claddings are chiral nihility media, in which the permittivity and permeability tend to be zero, the above parameters become $k_{1\pm} = \pm k_0\kappa_1$, $k_{2\pm} = n_2 k_0 = k_2$, $\gamma_{\pm} = (\beta^2 - k_{1\pm}^2)^{1/2} = (\beta^2 - k_0^2\kappa_1^2)^{1/2} = \gamma$, and $\delta_{\pm} = (k_2^2 - \beta^2)^{1/2} = \delta$. The dispersion relation given in (7) is divided into two equations as

$$(k_2^2-\beta^2)^{1/2}\frac{d}{2}=\tan^{-1}\left\{\frac{k_2}{k_0\kappa_1}\left(\frac{\beta^2-k_0^2\kappa_1^2}{k_2^2-\beta^2}\right)^{1/2}\right\}+m\pi,$$
$$m=0,\ 1,\ 2,\ \cdots \tag{9}$$

for RCP odd modes and

$$(k_2^2-\beta^2)^{1/2}\frac{d}{2}=-\tan^{-1}\left\{\frac{k_2}{k_0\kappa_1}\left(\frac{\beta^2-k_0^2\kappa_1^2}{k_2^2-\beta^2}\right)^{1/2}\right\}+m\pi,$$
$$m=1,\ 2,\ 3,\ \cdots \tag{10}$$

for LCP odd modes, where m is mode number. As can be seen, m starts from 0 in RCP odd modes and from 1 in LCP odd modes.

Also, the dispersion relation given in (8) is divided into two equations which take the form as

$$(k_2^2-\beta^2)^{1/2}\frac{d}{2}=-\tan^{-1}\left\{\frac{k_0\kappa_1}{k_2}\left(\frac{k_2^2-\beta^2}{\beta^2-k_0^2\kappa_1^2}\right)^{1/2}\right\}+m\pi,$$
$$m=1,\ 2,\ 3,\ \cdots \tag{11}$$

for RCP even modes and

$$(k_2^2-\beta^2)^{1/2}\frac{d}{2}=\tan^{-1}\left\{\frac{k_0\kappa_1}{k_2}\left(\frac{k_2^2-\beta^2}{\beta^2-k_0^2\kappa_1^2}\right)^{1/2}\right\}+m\pi,$$
$$m=0,\ 1,\ 2,\ \cdots \tag{12}$$

for LCP even modes. As can be seen, in contrast to odd modes, m starts from 1 in RCP odd modes and from 0 in LCP odd modes, because of the handedness of chiral meta-material.

2.3 Guided modes in chiral nihility claddings and NIM core waveguide

Consider that Region 1 and Region 3 shown in Fig. 1 are chiral nihility materials and the core is NIM. The dispersions (7) and (8) can be splited into two dispersion equations corresponding to two modes: RCP and LCP. The characteristic relation, cut-off frequencies, field profile, and energy in the different layers of the waveguide structure of RCP and LCP modes are found. We consider both odd and even modes.

2.3.1 Odd modes

Assume the core layer is negative-index material, thus the parameter n_2 has a negative value, so the dispersion relation given by (7) can be divided into two equations as

$$(k_2^2-\beta^2)^{1/2}\frac{d}{2}=\tan^{-1}\left\{\frac{k_2}{k_0\kappa_1}\left(\frac{\beta^2-k_0^2\kappa_1^2}{k_2^2-\beta^2}\right)^{1/2}\right\}+m\pi,$$
$$m=1,\ 2,\ 3,\ \cdots \tag{13}$$

for RCP odd modes and

$$(k_2^2-\beta^2)^{1/2}\frac{d}{2}=-\tan^{-1}\left\{\frac{k_2}{k_0\kappa_1}\left(\frac{\beta^2-k_0^2\kappa_1^2}{k_2^2-\beta^2}\right)^{1/2}\right\}+m\pi,$$
$$m=0,\ 1,\ 2,\ \cdots \tag{14}$$

for LCP odd modes. It is noted that, in contrast to (9) and (10), m starts from 0 in LCP odd modes and from 1 in RCP odd modes.

We can obtain the normalized cutoff frequencies (V) by setting $\beta\to k_0\kappa_1$ in the dispersion relations (13) and (14)

$$V=k_0d=\frac{2m\pi}{(n_2^2-\kappa_1^2)^{1/2}},\ m=1,\ 2,\ 3,\ \cdots \tag{15}$$

for RCP odd modes and

$$V=k_0d=\frac{2m\pi}{(n_2^2-\kappa_1^2)^{1/2}},\ m=0,\ 1,\ 2,\ \cdots \tag{16}$$

for LCP odd modes.

The derivation of the power flow (Poynting vector) is given in details in Appendix B for odd modes.

From Appendix B, the energy flow along the z-axis can be expressed as

$$S_z(x)=\begin{cases}\pm\dfrac{\beta k_0\kappa_1A^2\sin^2(u)}{\eta_2\gamma^2}\times\\ \exp\left\{-2\gamma\left(x-\dfrac{d}{2}\right)\right\},\ x>d/2\\ \dfrac{\beta k_2A^2}{\eta_2\delta^2}\cos^2(\delta x),\ -d/2\le x\le d/2\\ \pm\dfrac{\beta k_0\kappa_1A^2\sin^2(u)}{\eta_2\gamma^2}\times\\ \exp\left\{2\gamma\left(x+\dfrac{d}{2}\right)\right\},\ x<-d/2\end{cases} \tag{17}$$

for RCP (upper sign) and LCP (lower sign) odd modes.

Inspection of (17) reveals that S_z is positive for RCP odd modes and negative for LCP odd modes in the surroundings, and positive for both RCP and LCP odd modes in the guiding layer. On the other hand, we use NIM guiding layer which makes the energy flux negative for both RCP and LCP odd modes.

2.3.2 Even modes

We again assume a NIM in the core of negative index n_2, so the dispersion relation given in (8) can be divided into two equations as

$$(k_2^2-\beta^2)^{1/2}\frac{d}{2}=-\tan^{-1}\left\{\frac{k_0\kappa_1}{k_2}\left(\frac{k_2^2-\beta^2}{\beta^2-k_0^2\kappa_1^2}\right)^{1/2}\right\}+m\pi,$$

$$m=0,\ 1,\ 2,\ \cdots \tag{18}$$

for RCP even modes and

$$(k_2^2-\beta^2)^{1/2}\frac{d}{2}=\tan^{-1}\left\{\frac{k_0\kappa_1}{k_2}\left(\frac{k_2^2-\beta^2}{\beta^2-k_0^2\kappa_1^2}\right)^{1/2}\right\}+m\pi,$$

$$m=1,\ 2,\ 3,\ \cdots \tag{19}$$

for LCP even modes.

We can obtain the normalized cutoff frequencies (V) by setting $\beta\to k_0\kappa_1$ in the dispersion (18) and (19)

$$V=k_0d=\frac{(2m+1)\pi}{(n_2^2-\kappa_1^2)^{1/2}},\ m=0,\ 1,\ 2,\ \cdots \tag{20}$$

for RCP even modes and

$$V=k_0d=\frac{(2m-1)\pi}{(n_2^2-\kappa_1^2)^{1/2}},\ m=1,\ 2,\ 3,\ \cdots \tag{21}$$

for LCP even modes.

The derivation of the power flow (Poynting vector) is given in details in Appendix C for even modes. From Appendix C, the enery flow along the z-axis can be expressed as

$$S_z(x)=\begin{cases}\pm\dfrac{\beta k_0\kappa_1 A^2\cos^2(u)}{\eta_2\gamma^2}\times\\ \exp\left\{-2\gamma\left(x-\dfrac{d}{2}\right)\right\},\ x>d/2\\ \dfrac{\beta k_2A^2}{\eta_2\delta^2}\sin^2(\delta x),\ -d/2\le x\le d/2\\ \pm\dfrac{\beta k_0\kappa_1 A^2\cos^2(u)}{\eta_2\gamma^2}\times\\ \exp\left\{2\gamma\left(x+\dfrac{d}{2}\right)\right\},\ x<-d/2\end{cases} \tag{22}$$

for RCP (upper sign) and LCP (lower sign) even modes, respectively. It is obvious from (22) that S_z is positive for RCP even modes and negative for LCP even modes in the cladding, and positive for both RCP and LCP even modes in the core. On the other hand, we use the NIM core which makes the energy flux negative in the core for both RCP and LCP even modes.

3. Results and discussion

We can calculate the propagation constants numerically from the dispersion relations (13), (14), (18), and (19), then the electromagnetic fields and the energy flow distribution can be calculated. In this section, we use numerical values for the parameters in the core and cladding as $\mu_1=\varepsilon_1=0$, $\kappa_1=0.1$, $\mu_2=(-5+.001\mathrm{i})\times\mu_0$, $\varepsilon_2=(-5+.001\mathrm{i})\times\varepsilon_0$, and $\kappa_2=0$.

3.1 Dispersion curves

The dispersion properties of odd and even guided low-order modes are illustrated in Fig. 2, where $n_{\text{eff}}=\beta/k_0$ is the modal refractive index, and k_0d is the normalized thickness or frequency. We assume chiral nihility madium in the surroundings and NIM guiding layer waveguide structuture. The odd and even modes are represented by dashed and solid curves, respectively. For LCP

odd and even modes, the dispersion curves increase monotonically. The effective refractive index incerases monotonically with the normalized frequency. The normalized cutoff frequencies (points C_1 and C_2 where $n_{\text{eff}}=1$) satisfy (16) or (21). However, for RCP odd and even modes, the dispersion curves are no longer increasing monotonically, but are bent. The cutoff frequencies where $n_{\text{eff}}=1$ are not the minimum frequencies that waves can propagate. Considering the fundamnetal mode where $m=0$, there is one solution below cutoff frequency (Point C_1) for RCP even mode in some frequency region. If we consider the first guided mode, $m=1$, there exist two solutions below cutoff frequencies (Points C_2 and C_3) for both RCP even and odd modes in some frequency region. Therefore, the cutoff frequencies are no longer really "cutoff". The real "cutoff" frequencies correspond to the minimum frequencies (critical Points *B* and *D*) that guided wave can propagate. As the normalized frequency increases from the critical Points *B* and *D*, dispersion curves split into two branches, which the modal index increases with an increase in the normalized frequency for upper branch and decreases to $n_{\text{eff}}=1$ for lower branch.

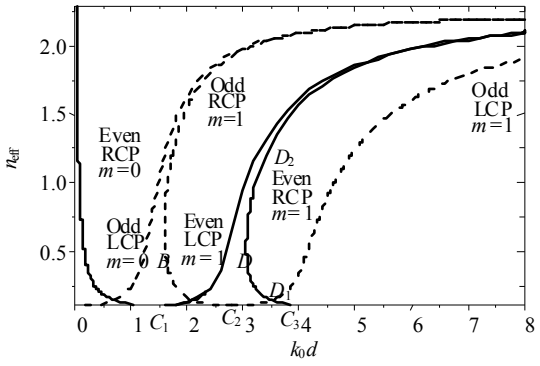

Fig. 2 Dispersion curves of guided modes in the chiral nihility cladding and negative-index material core waveguide.

3.2 Odd guided modes

The field profile which shows the amplitudes of electric and magnetic fields is illustrated in Fig. 3 at normalized thichness $k_0d=2.2$ for RCP odd first mode. Figure 4 illustrates the energy flux distribution at normalized thichness $k_0d=2.2$ for RCP odd first mode. As can be seen from Fig. 3, E_z and H_z are odd functions of x (sin form) and E_x, E_y, H_x, and H_y (cos form) are even functions of x. S_z is positive in the cladding and is negative in the core due to the NIM core material. However, there are two propagation constants at $k_0d=2.2$.

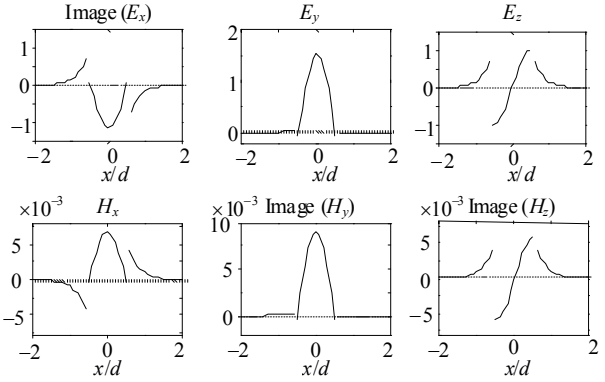

Fig. 3 Amplitudes of electromagnetic field components at $k_0d=2.2$ for RCP odd mode when $m=1$, $n_{\text{eff}}=1.6921$.

The field profile is plotted in Fig. 5 whereas and energy flux distribution is shown in Fig. 6 at normalized thickness $k_0d=2$ for LCP odd fundamental mode. As Fig. 5 shows, E_z and H_z are odd functions of x (sin form), and E_x, E_y, H_x, and H_y (cos form) are even functions of x. As can be seen from Fig. 6, S_z is negative in both the guiding layer and the surroundings due to the negative refractive index of the guiding layer.

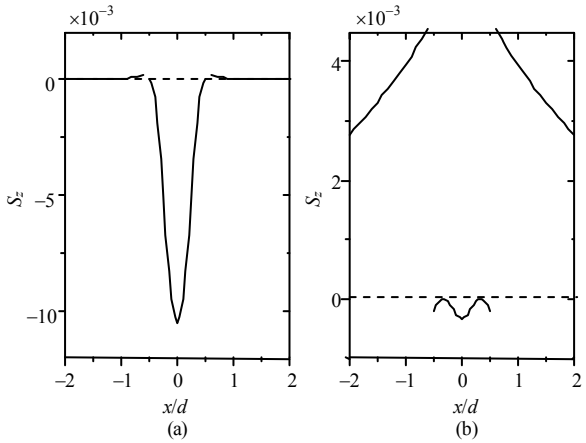

Fig. 4 Energy flux at $k_0d=2.2$ for RCP odd mode when $m=1$: (a) $n_{\text{eff}}=1.6921$ and (b) $n_{\text{eff}}=0.1284$.

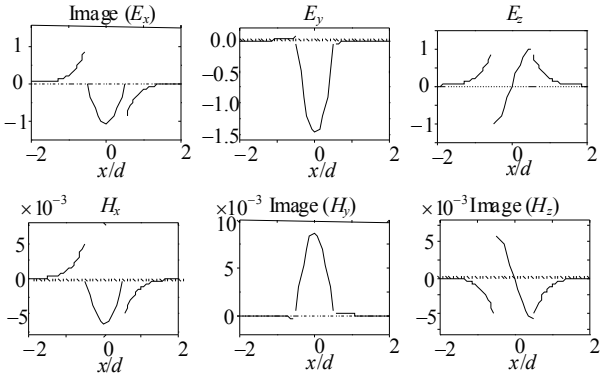

Fig. 5 Field profiles at $k_0d = 2$ for LCP odd fundamental mode.

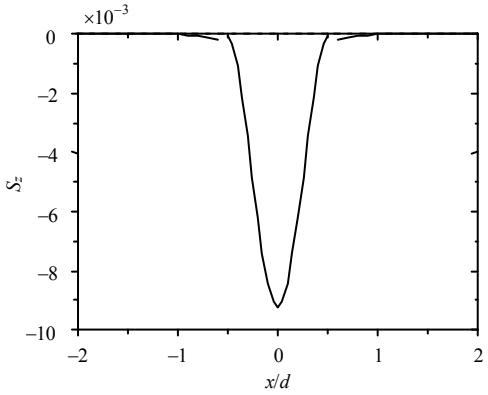

Fig. 6 Energy flux at $k_0d = 2$ for LCP odd mode when $m = 0$.

3.3 Even guided modes

The field profile is plotted in Fig. 7 whereas the energy flux distribution is shown in Fig. 8 at $k_0d = 0.5$ for RCP even fundamental mode. As clearly shown in Fig. 7, E_z and H_z are even functions of x (cos form), and E_x, E_y, H_x, and H_y are odd functions of x (sin form). It is obvious from Fig. 8 that S_z is positive in the surroundings and is negative in the guiding layer as expected.

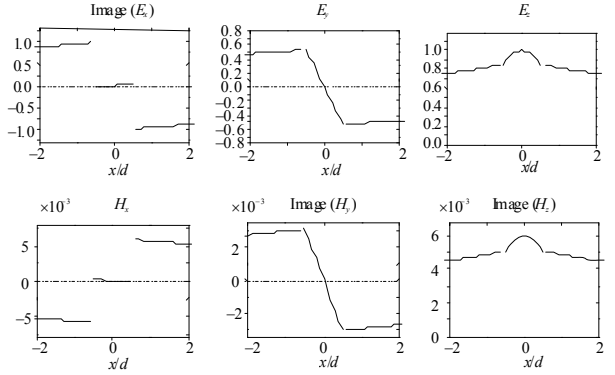

Fig. 7 Field profiles at $k_0d = 0.5$ for RCP even fundamental mode.

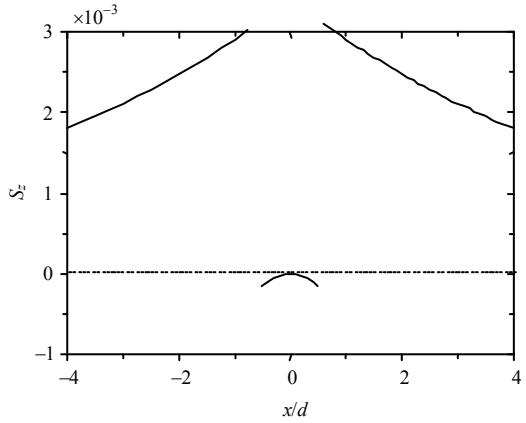

Fig. 8 Energy flux at $k_0d = 0.5$ for RCP even mode when $m = 0$.

The field profils are shown in Fig. 9, and the energy flux distribution is illustrated in Fig. 10 at $k_0d = 3$ for LCP even first mode. As clearly seen from Fig. 9, E_z and H_z are even functions of x (cos form), and E_x, E_y, H_x, and H_y (sin form) are odd functions of x. As can be seen from Fig. 10, S_z is negative in both the guiding layer and the surroundings.

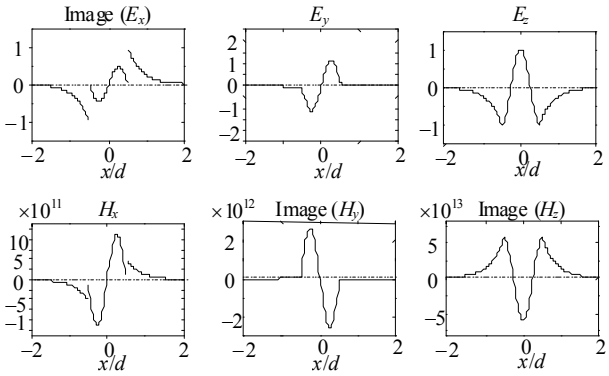

Fig. 9 Amplitudes of electromagnetic field components at $k_0d = 3$ for LCP even mode when $m = 1$.

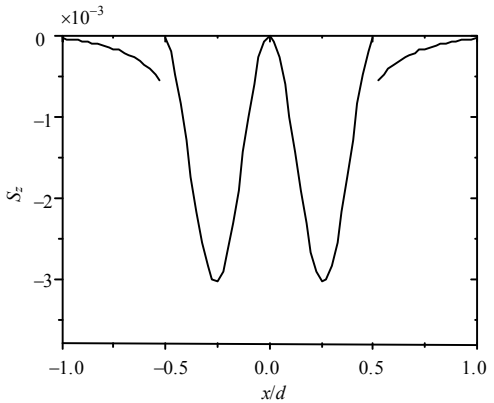

Fig. 10 Energy flux at $k_0d = 3$ for LCP even mode when $m = 1$.

4. Conclusions

The dispersion equations of three-layer asymmetric and symmetric chiral slab waveguides are derived. We first assume the three layers are chiral media. Guided modes in a special case of chiral nihility claddings, and NIM core waveguides are presented in details. Both the dispersion equations for odd and even RCP and LCP guided modes in the chiral nihility waveguides are examined. For odd and even guided modes, the dispersion relations, normalized cutoff frequencies, field profiles, and energy flow of RCP and LCP modes are derived and plotted. A numerical results for typical chirality parameters of several guided modes are given. Some novel features such as abnormal dispersion curves in the chiral nihility waveguides are mentioned.

Appendix A

The solutions of the longitudinal-field component in (4) can be written as

$$E_{z\pm}(x)=\begin{cases} A_{\pm}\exp\left(-\gamma_{\pm}\left(x-\dfrac{d}{2}\right)\right), & x>d/2 \\ B_{\pm}\sin\left(\delta_{\pm}x\right), & -d/2\le x\le d/2 \\ C_{\pm}\exp\left(\alpha_{\pm}\left(x+\dfrac{d}{2}\right)\right), & x<-d/2 \end{cases} \tag{1A}$$

for odd guided modes and

$$E_{z\pm}(x)=\begin{cases} A_{\pm}\exp\left(-\gamma_{\pm}\left(x-\dfrac{d}{2}\right)\right), & x>d/2 \\ B_{\pm}\cos\left(\delta_{\pm}x\right), & -d/2\le x\le d/2 \\ C_{\pm}\exp\left(\alpha_{\pm}\left(x+\dfrac{d}{2}\right)\right), & x<-d/2 \end{cases} \tag{2A}$$

for even guided modes, where the parameters $\gamma_{\pm}$, $\delta_{\pm}$, and $\alpha_{\pm}$ are given be $\gamma_{\pm}=(\beta^2-k_{1\pm}^2)^{1/2}$, $\delta_{\pm}=(k_{2\pm}^2-\beta^2)^{1/2}$, and $\alpha_{\pm}=(\beta^2-k_{3\pm^2})^{1/2}$.

The other field components can be obtained by using (2), (3), and (4). Applying the continuity requirement of electromagnetic field components at $x=d/2$ and $x=-d/2$, the dispersion relations of guided modes in three-layer slab chiral waveguide can be derived as

$$\begin{aligned} &\frac{4\gamma_{+}k_{2+}k_{2-}}{\delta_{-}}\left(\frac{\eta_2-\eta_1}{\eta_3}\right)\cos u_{+}\cos u_{-}+ \\ &4\left(\frac{\eta_2-\eta_1}{\eta_3}\right)\left(k_{1+}k_{2+}\right)\sin u_{-}\cos u_{+}+\gamma_{+}k_{2+}\left(1+\frac{\eta_2}{\eta_3}\right)\times \\ &\left(1-\frac{\eta_2}{\eta_3}\right)\left(1+\frac{\eta_1}{\eta_2}\right)\left(\frac{k_{3-}}{\alpha_{-}}+\frac{k_{3+}}{\alpha_{+}}\right)\sin u_{-}\cos u_{+}- \\ &\left\{\frac{k_{3-}}{\alpha_{-}}\left(1-\frac{\eta_2}{\eta_3}\right)^2+\frac{k_{3+}}{\alpha_{+}}\left(1+\frac{\eta_2}{\eta_3}\right)^2\right\}\times \\ &\left(1-\frac{\eta_1}{\eta_2}\right)\left(\frac{\gamma_{+}\delta_{+}k_{2-}}{\delta_{-}}\right)\cos u_{-}\sin u_{+}- \\ &\left\{2\frac{k_{3-}}{\alpha_{-}}\left(1-\frac{\eta_2}{\eta_3}\right)\left(1+\frac{\eta_1}{\eta_3}\right)+2\frac{k_{3+}}{\alpha_{+}}\left(1+\frac{\eta_2}{\eta_3}\right)\left(1-\frac{\eta_1}{\eta_3}\right)\right\}\times \\ &\delta_{+}k_{1+}\sin u_{+}\sin u_{-}=0 \end{aligned} \tag{3A}$$

for odd guided modes and

$$\begin{aligned} &\frac{-4\gamma_{+}k_{2+}k_{2-}}{\delta_{-}}\left(\frac{\eta_2-\eta_1}{\eta_3}\right)\sin u_{+}\sin u_{-}+ \\ &4\left(\frac{\eta_2-\eta_1}{\eta_3}\right)\left(k_{1+}k_{2+}\right)\cos u_{-}\sin u_{+}+\gamma_{+}k_{2+}\left(1+\frac{\eta_2}{\eta_3}\right)\times \\ &\left(1-\frac{\eta_2}{\eta_3}\right)\left(1+\frac{\eta_1}{\eta_2}\right)\left(\frac{k_{3-}}{\alpha_{-}}+\frac{k_{3+}}{\alpha_{+}}\right)\cos u_{-}\sin u_{+}- \\ &\left\{\frac{k_{3-}}{\alpha_{-}}\left(1-\frac{\eta_2}{\eta_3}\right)^2+\frac{k_{3+}}{\alpha_{+}}\left(1+\frac{\eta_2}{\eta_3}\right)^2\right\}\times \\ &\left(1-\frac{\eta_1}{\eta_2}\right)\left(\frac{\gamma_{+}\delta_{+}k_{2-}}{\delta_{-}}\right)\sin u_{-}\cos u_{+}+ \\ &\left\{2\frac{k_{3-}}{\alpha_{-}}\left(1-\frac{\eta_2}{\eta_3}\right)\left(1+\frac{\eta_1}{\eta_3}\right)+2\frac{k_{3+}}{\alpha_{+}}\left(1+\frac{\eta_2}{\eta_3}\right)\left(1-\frac{\eta_1}{\eta_3}\right)\right\}\times \\ &\delta_{+}k_{1+}\cos u_{+}\cos u_{-}=0 \end{aligned} \tag{4A}$$

for even guided modes, where $u_{\pm}=\delta_{\pm}d/2$.

When the structure shown in Fig. 1 becomes symmetric, i.e., $\kappa_1=\kappa_3$, $\varepsilon_1=\varepsilon_3$, and $\mu_1=\mu_3$, the solutions of the longitudinal-field component in (4) are now written as

$$E_{z\pm}(x)=\begin{cases} A_{\pm}\exp\left(-\gamma_{\pm}\left(x-\dfrac{d}{2}\right)\right), & x>d/2 \\ B_{\pm}\sin\left(\delta_{\pm}x\right), & -d/2\le x\le d/2 \\ A_{\pm}\exp\left(\gamma_{\pm}\left(x+\dfrac{d}{2}\right)\right), & x<-d/2 \end{cases} \tag{5A}$$

for odd guided modes and

$$E_{z\pm}(x)=\begin{cases}A_{\pm}\exp\left(-\gamma_{\pm}\left(x-\dfrac{d}{2}\right)\right), & x\geq d/2\\ B_{\pm}\cos\left(\delta_{\pm}x\right), & -d/2<x<d/2\\ A_{\pm}\exp\left(\gamma_{\pm}\left(x+\dfrac{d}{2}\right)\right), & x\leq -d/2\end{cases} \tag{6A}$$

for even guided modes.

Other components of the fields are obtained, the continuity conditions are applied, and we obtain the following dispersion relations

$$\frac{4k_{2+}k_{2-}}{\delta_{+}\delta_{-}}\cos u_{+}\cos u_{-}+\frac{4k_{1+}k_{1-}}{\gamma_{+}\gamma_{-}}\sin u_{+}\sin u_{-}-\left(\frac{1}{\eta_1\eta_2}\right)\left\{\left[\frac{k_{1+}k_{2+}}{\delta_{+}\gamma_{+}}(\eta_1-\eta_2)^2+\frac{k_{1-}k_{2+}}{\delta_{+}\gamma_{-}}(\eta_1+\eta_2)^2\right]\sin u_{-}\cos u_{+}+\left[\frac{k_{1-}k_{2-}}{\delta_{-}\gamma_{-}}(\eta_1-\eta_2)^2+\frac{k_{1+}k_{2-}}{\delta_{-}\gamma_{+}}(\eta_1+\eta_2)^2\right]\cos u_{-}\sin u_{+}\right\}=0 \tag{7A}$$

for odd guided modes and

$$\frac{4k_{1+}k_{1-}}{\gamma_{+}\gamma_{-}}\cos u_{+}\ \text{relations}\ \cos u_{-}+\frac{4k_{2+}k_{2-}}{\delta_{+}\delta_{-}}\sin u_{+}\sin u_{-}+\left(\frac{1}{\eta_1\eta_2}\right)\times\left\{\left[\frac{k_{1+}k_{2-}}{\delta_{-}\gamma_{+}}(\eta_1+\eta_2)^2+\frac{k_{1-}k_{2-}}{\delta_{-}\gamma_{-}}(\eta_1-\eta_2)^2\right]\sin u_{-}\cos u_{+}+\left[\frac{k_{1-}k_{2+}}{\delta_{+}\gamma_{-}}(\eta_1+\eta_2)^2+\frac{k_{1+}k_{2+}}{\delta_{+}\gamma_{+}}(\eta_1-\eta_2)^2\right]\cos u_{-}\sin u_{+}\right\}=0 \tag{8A}$$

for even guided modes.

Appendix B

We now derive the energy flow (Poynting vector) in RCP and LCP odd modes.

We can express the electromagnetic fields in explicit forms as

$$E_x(x)=\begin{cases}-\dfrac{\mathrm{j}\beta A\sin(u)}{\gamma}\exp\left\{-\gamma\left(x-\dfrac{d}{2}\right)\right\}, & x>d/2\\ -\dfrac{\mathrm{j}\beta A}{\delta}\cos(\delta x), & -d/2\leq x\leq d/2\\ +\dfrac{\mathrm{j}\beta A\sin(u)}{\gamma}\exp\left\{\gamma\left(x+\dfrac{d}{2}\right)\right\}, & x<-d/2\end{cases} \tag{1B}$$

$$E_y(x)=\begin{cases}-\dfrac{k_0\kappa_1 A\sin(u)}{\gamma}\exp\left\{-\gamma\left(x-\dfrac{d}{2}\right)\right\}, & x>d/2\\ \mp\dfrac{k_2 A}{\delta}\cos(\delta x), & -d/2\leq x\leq d/2\\ +\dfrac{k_0\kappa_1 A\sin(u)}{\gamma}\exp\left\{\gamma\left(x+\dfrac{d}{2}\right)\right\}, & x<-d/2\end{cases} \tag{2B}$$

and

$$E_z(x)=\begin{cases}A\sin(u)\exp\{-\gamma(x-d/2)\}, & x>d/2\\ A\sin(\delta x), & -d/2\leq x\leq d/2\\ A\sin(u)\exp\{\gamma(x+d/2)\}, & x<-d/2.\end{cases} \tag{3B}$$

The minus sign (upper) corrsponds to RCP odd modes whereas the positive sign (lower) corrsponds to LCP odd modes. A is a constant.

The magnetic fields can be calculted in the different layers through the relation

$$H_{x,y,z}=\pm\frac{\mathrm{j}}{\eta_2}E_{x,y,z} \tag{4B}$$

for RCP (upper sign) and LCP (lower sign) odd modes.

The energy flow is simply given by the Poynting vector

$$S_z=\frac{1}{2}\mathrm{Re}\left(E\times H^{*}\right)=\frac{1}{2}\mathrm{Re}\left(E_xH_y^{*}-E_yH_x^{*}\right) \tag{5B}$$

Thus we can express the energy flow along the *z*-axis as

$$S_z(x)=\begin{cases}\pm\dfrac{\beta k_0\kappa_1 A^2\sin^2(u)}{\eta_2\gamma^2}\exp\left\{-2\gamma\left(x-\dfrac{d}{2}\right)\right\}, & x>d/2\\ \dfrac{\beta k_2 A^2}{\eta_2\delta^2}\cos^2(\delta x), & -d/2\leq x\leq d/2\\ \pm\dfrac{\beta k_0\kappa_1 A^2\sin^2(u)}{\eta_2\gamma^2}\exp\left\{2\gamma\left(x+\dfrac{d}{2}\right)\right\}, & x<-d/2\end{cases} \tag{6B}$$

for RCP (upper sign) and LCP (lower sign) odd modes.

Appendix C

We now derive the energy flow (Poynting vector) in RCP and LCP even modes.

We can express the electromagnetic fields in explicit forms as

$$E_x(x)=\begin{cases}-\dfrac{\mathrm{j}\beta A\cos(u)}{\gamma}\exp\left\{-\gamma\left(x-\dfrac{d}{2}\right)\right\}, & x>d/2\\ +\dfrac{\mathrm{j}\beta A}{\delta}\sin(\delta x), & -d/2\le x\le d/2\\ +\dfrac{\mathrm{j}\beta A\cos(u)}{\gamma}\exp\left\{\gamma\left(x+\dfrac{d}{2}\right)\right\}, & x<-d/2\end{cases} \quad (1C)$$

$$E_y(x)=\begin{cases}-\dfrac{k_0\kappa_1 A\cos(u)}{\gamma}\exp\left\{-\gamma\left(x-\dfrac{d}{2}\right)\right\}, & x>d/2\\ \pm\dfrac{k_2 A}{\delta}\sin(\delta x), & -d/2\le x\le d/2\\ +\dfrac{k_0\kappa_1 A\cos(u)}{\gamma}\exp\left\{\gamma\left(x+\dfrac{d}{2}\right)\right\}, & x<-d/2\end{cases} \quad (2C)$$

$$E_z(x)=\begin{cases}A\cos(u)\exp\left\{-\gamma\left(x-\dfrac{d}{2}\right)\right\}, & x>d/2\\ A\cos(\delta x), & -d/2\le x\le d/2\\ A\cos(u)\exp\left\{\gamma\left(x+\dfrac{d}{2}\right)\right\}, & x<-d/2\end{cases} \quad (3C)$$

for RCP (upper sign) and LCP (lower sign) even modes.

The magnetic fields in the core and the cladding are given by (4B). We can express the energy flow along the z-axis in the waveguide as

$$S_z(x)=\begin{cases}\pm\dfrac{\beta k_0\kappa_1 A^2\cos^2(u)}{\eta_2\gamma^2}\exp\left\{-2\gamma\left(x-\dfrac{d}{2}\right)\right\}, & x>d/2\\ \dfrac{\beta k_2 A^2}{\eta_2\delta^2}\sin^2(\delta x), & -d/2\le x\le d/2\\ \pm\dfrac{\beta k_0\kappa_1 A^2\cos^2(u)}{\eta_2\gamma^2}\exp\left\{2\gamma\left(x+\dfrac{d}{2}\right)\right\}, & x<-d/2.\end{cases} \quad (4C)$$

for RCP (upper sign) and LCP (lower sign) even modes, respectively.

References

[1] V. Veselago, "The electrodynamics of substances with simultaneously negative values of ε and μ," *Soviet Physics Uspekhi*, 1968, 10(4): 509–514.

[2] H. M. Kullab, I. M. Qadoura, and S. A. Taya, "Slab waveguide sensor with left-handed material core layer for detection an adlayer thickness and index," *Journal of Nano-and Electronic and Physics*, 2015, 7(2): 1–6.

[3] H. Chen, B. I. Wu, and J. A. Kong, "Review of electromagnetic theory in left-handed materials," *Journal of Electromagnetic Waves & Applications*, 2006, 20(15): 2137–2151.

[4] S. A. Taya, E. J. El-Farram, and M. M. Abadla, "Symmetric multilayer slab waveguide structure with a negative index material: TM case," *Optik – Internal Journal for Light and Electron Optics*, 2012, 123(24): 2264–2268.

[5] S. A. Taya and I. M. Qadoura, "Guided modes in slab waveguides with negative index cladding and substrate," *Optik – Internal Journal for Light and Electron Optics*, 2013, 124(13): 1431–1436.

[6] C. W. Qiu, L. W. Li, N. Burokur, and S. Zouhd, "Chiral nihility effects on energy flow in chiral materials," *Journal of the Optical Society of America A: Optics Image Science & Vision*, 2008, 25(1): 55–63.

[7] S. A. Taya and K. Y. Elwasife, "Guided modes in a metal-clad waveguide comprising a left-handed material as a guiding layer," *International Journal of Research & Reviews in Applied Sciences*, 2012, 13(1): 294–305.

[8] S. A. Taya, K. Y. Elwasife, and H. M. Kullab, "Dispersion properties of anisotropic-metamaterial slab waveguide structure," *Optica Applicata*, 2013, 43(4): 857–869.

[9] J. B. Pendry, "Negative refraction makes a perfect lens," *Physical Review Letters*, 2000, 85(18): 3966–3969.

[10] I. Qadoura, S. Taya, and K. El-Wasife, "Scaling rules for a slab waveguide structure comprising nonlinear and negative index materials," *International Journal of Microwave & Optical Technology*, 2012, 7(5): 349–357.

[11] J. B. Pendry, A. J. Holden, D. J. Robbins, and W. J. Stewart, "Magnetism from conductors and enhanced nonlinear phenomena," *IEEE Transactions on Microwave Theory and Techniques*, 1999, 47(11): 2075–2084.

[12] M. M. Abadla and S. A. Taya, "Characteristics of left-handed multilayer slab waveguide structure," *The Islamic University Journal* (*Series of Natural Studies and Engineering*), 2011, 19(1): 57–70.

[13] J. B. Pendry, A. J. Holden, D. J. Robbins, and W. J. Stewart, "Low frequency plasmons in thin-wire structures," *Journal of Physics-Condensed Matter*, 1998, 1(22): 4785–4809.

[14] S. A. Taya, H. M. Kullab, and I. M. Qadoura, "Dispersion properties of slab waveguides with double negative material guiding layer and nonlinear substrate," *Journal of the Optical Society of America B: Optical Physics*, 2013, 30(7): 2008–2013.

[15] A. Gribe and G. V. Eleftheriades, "Growing evanescent waves in negative-refractive index," *Applied Physics Letters*, 2003, 82(12): 1815–1817.

[16] M. M. Abadla and S. A. Taya, "Excitation of TE surface polaritons in different structures comprising a left-handed material and a metal," *Optik – Internal Journal for Light and Electron Optics*, 2014, 125(3): 1401–1405.

[17] D. K. Qing and G. Chen, "Enhancement of evanescent waves in waveguides using metamaterials of negative permittivity and permeability," *Applied Physics Letters*, 2004, 84(5): 669–671.

[18] S. A. Taya and K. Y. Elwasife, "Field profile of asymmetric slab waveguide structure with LHM layers," *Journal Nano-and Electronic Physics*, 2014, 6(2): 02007-1–02007-5.

[19] A. Alu and N. Engheta, "Achieving transparency with plasmonic and metamaterial coatings," *Physical Review E: Statistical Nonlinear & Soft Matter Physics*, 2005, 72: 016623-1–016623-10.

[20] S. A. Taya, "Dispersion properties of lossy, dispersive, and anisotropic left-handed material slab waveguide," *Optik – Internal Journal for Light and Electron Optics*, 2015, 126(4): 1319–1323.

[21] S. A. Taya and D. M. Alamassi, "Reflection and transmission from left-handed material structures using Lorentz and Drude medium models," *Opto-Electronics Review*, 2015, 23(3): 214–221.

[22] B. J. Lee, C. Fu, K. Park, and Z. M. Zhang, "Study of the surface and bulk polaritons with a negative index metamaterial," *Journal of the Optical Society of America B: Optical Physic*, 2005, 22(5): 1016–1023.

[23] R. Shelby, D. Smith, and S. Schultz, "Experimental verification of a negative index of refraction," *Science*, 2001, 292(5514): 77–79.

[24] T. Ergin, N. Stenger, P. Brenner, J. B. Pendry, and M. Wegener, "Three-dimensional invisibility cloak at optical wavelengths," *Science*, 2010, 328(5976): 337–339.

[25] L. W. Li, Y. N. Li, T. S. Yeo, J. R. Mosig, and O. J. F. Martin, "A broadband and high-gain metamaterial microstrip antenna," *Applied Physics Letters*, 2010, 96(16): 164–165.

[26] Z. H. Zhang, Z. P. Wang, and L. H. Wang, "Design principle of single- or double-layer wave-absorbers containing left-handed materials," *Materials and Design*, 2009, 30(9): 3908–3912.

[27] H. Kullab, S. Taya, and T. El-Agez, "Metal-clad waveguide sensor using a left-handed material as a core layer," *Journal of the Optical Society of America B: Optical Physics*, 2102, 29(5): 959–964.

[28] H. M. Kullab and S. A. Taya, "Peak type metal-clad waveguide sensor using negative index materials," *AEU – Internayional Journal Electronics Communications*, 2013, 67(11): 905–992.

[29] H. M. Kullab and S. A. Taya, "Transverse magnetic peak type metal-clad optical waveguide sensor," *Optik – Internal Journal for Light and Electron Optics*, 2014, 125(1): 97–100.

[30] S. A. Taya and H. M. Kullab, "Optimization of transverse electric peak type metal-clad waveguide sensor using double negative materials," *Applied Physics A*, 2014, 116(4): 1841–1846.

[31] S. A. Taya, "Slab waveguide with air core layer and anisotropic left-handed material claddings as a sensor," *Opto-Electronics Review*, 2014, 22(4): 252–257.

[32] S. A. Taya, "P-polarized surface waves in a slab waveguide with left-handed material for sensing applications," *Journal of Magnetism & Magnetic Materials*, 2015, 377: 281–285.

[33] S. A. Taya, "Theoretical investigation of slab waveguide sensor using anisotropic metamaterials," *Optica Applicata*, 2015, 45(3): 405–417.

[34] S. A. Taya, A. A. Jarada, and H. M. Kullab, "Slab waveguide sensor utilizing left-handed material core and substrate layers," *Optik – Internal Journal for Light and Electron Optics*, 2016, 127(19): 7732–7739.

[35] S. A. Taya, S. S. Mahdi, A. A. Alkanoo, and I. M. Qadoura, "Slab waveguide with conducting interfaces as an efficient optical sensor: TE case," *Optica Acta International Journal of Optics*, 2017, 64(8): 836–843.

[36] S. A. Taya, S. A. Shaheen, and A. A. Alkanoo, "Photonic crystal as a refractometric sensor operated in reflection mode," *Superlattices and Microstructures*, 2017, 101: 299–305.

[37] J. F. Dong and C. Xu, "Characteristics of guided modes in planner chiral nihility meta-material waveguides," *Progress In Electromagnetic Research*

B, 2009, 14: 107–126.

[38] P. Pelet and N. Engheta, "The theory of chirowaveguides," *IEEE Transactions on Antennas and Propagation*, 1990, 38(1): 90–98.

[39] M. Oksanen, P. Kolivisto, and I. lindell, "Dispersion curves and fields for a chiral slab waveguide," *IEEE Proceedings H-Microwaves, Antennas and Propagation*, 1991, 138(4): 327–344.

[40] J. Xiao, K. Zhang, and L. Gong, "Field analysis of a general chiral planer waveguide," *International Journal of lnfrared and Millimeter Waves*, 1997, 18(4): 939–948.

[41] M. Yokota and Y. Yamanaka, "Dispersion relation and field distribution for a chiral slab waveguide," *International Journal of Microwave and Optical Technology*, 2006, 1: 623–627.

[42] R. Zhao, T. Koschny, and C. M. Soukoulis, "Chiral metamaterials: retrieval of the effective parameters with and without substrate," *Optics Express*, 2010, 18(14): 553–567.

[43] J. F. Dong and J. Li, "Characteristics of guided modes in uniaxial chiral circular waveguides," *Progress In Electromagnetics Research*, 2012, 124(124): 331–345.